Determining elastic constants of an orthorhombic material by physical seismic modeling

Faranak Mahmoudian, Gary F. Margrave, P. F. Daley, Joe Wong, and Eric Gallant

ABSTRACT

Vertically fractured media are commonly described by an HTI (horizontal transverse isotropy) model, which is a degenerate case of the more general orthorhombic symmetry. To study the seismic effects of such a medium, a model from phenolic LE material, which exhibits the orthorhombic symmetry, was constructed. To characterize the anisotropy of the phenolic model the set of nine elastic constants is determined. Elastic constants are most often found from measurements of the phase velocity in a variety of directions, but finding this plane-wave velocity is problematic. Instead of the phase velocity, group velocity, which can be measured easily and more reliably, is used. Scaled physical modeling experiments in the laboratory in which ultrasonic elastic waves are propagated through the phenolic model are used to measure the P- and S-wave group velocity in different directions in the principal planes. A linear expression between the P-wave group velocity in an arbitrary direction and elastic constants, has allowed us to estimate all nine elastic constants. Although actually slightly orthorhombic, the phenolic model exhibits approximate HTI symmetry requiring only five elastic constants to characterize the medium.

INTRODUCTION

Both academia and industry have tried to use laboratory measurements including ultrasonic wavespeed measurements or physical modeling scaled seismic data, for determination of the elastic constants (stiffnesses, C_{ij}) of anisotropic solids. Elastic constants characterize the anisotropy of a material which is essential when processing seismic data. When conventional seismic processing does not take anisotropy into account the earth is poorly imaged (Vestrum et al., 1999) leading to erroneous interpretations of the structure of the earth and a lower likelihood of finding oil and gas.

Elastic constants of layered rocks can be measured using the pulse through transmission technique on sets of cylindrical cores cut at particular angles of 0°, 90°, and 45° to the layering to determine elastic constants of the orthorhombic material, as employed in the work of a number of researcher (e.g., Cheadle et al. (1991); Dellinger and Vernik (1994); Vernik and Nur (1992); Lo et al. (1986); Jones and Wang (1981)). In this method, transducers are attached to the flat ends of the cores and the firstbreak traveltimes of P, SV, and SH-waves are measured. Using the relation between the phase velocity and elastic constants, the set of orthorhombic elastic constants are fit to the results. Every and Sachse (1992) used a least-squares fitting procedure to obtain combinations of elastic constants $(C_{23} + 2C_{44}), (C_{13} + 2C_{55})$, and $(C_{12} + 2C_{66})$ from the P-wave phase velocities measured in a number of non-symmetric directions. Mah and Schmitt (2001) employing the $\tau - p$ transform, measured the phase velocities in a variety of directions in an orthorhombic material to determine the nine elastic constants. Mah and Schmitt (2002) extended their method to determine the complete set of 21 elastic constants in a general anisotropic material, while assuming no a priori information about the symmetry of the material or

orientation of the summery axes. In the above mentioned experiments, the essential assumption is that the recorded firstbreaks represented phase velocities. However, the phase (plane-wave) velocities are sometimes difficult to measure experimentally. In the transmission experiment, traveltime measurements yield the phase velocity if the transducers are relatively wide compared to their separation, or the group velocity if the transducers are very small compared to their separation (Dellinger and Vernik, 1994; Vestrum, 1994; Auld, 1973). For an experiment with a source-receiver separation three times greater than the transducer width, Dellinger and Vernik (1994) concluded that the experiments of this kind should measure anisotropic phase velocity, not group velocity. The only possible way to record phase velocity in a transmission experiment is to have the source and receiver transducer width comparable to the source-receiver distance in order for the plane wave assumption to be valid. Nevertheless, finding the phase (plane-wave) velocity is problematic; due to the small size of sample there are rather large errors associated with picking the firstbreak and consequently may result in phase velocity measurements with high error. Not being able to measure phase velocities substantially complicates the determination of elastic constants in pulse transmission measurements (Vestrum et al., 1999; Mah and Schmitt, 2001). With so much research done on this subject, experimentally determining the nine independent elastic constants of the orthorhombic symmetry material remains challenging (Mah and Schmitt, 2001). One approach to reduce the associated errors of elastic constants is to measure the group velocity instead of the phase velocity.

In transmission experiments on a model with large enough dimensions, the measured firstbreak determines the group velocity, which is not equal to the phase velocity except for the principal directions. The group velocity, the velocity of energy propagation, is easier to measure and most likely to be found in an transmission experiment. Cheadle et al. (1991) used the P-wave group velocity measured in the direction of 45° to principal axes to determine the off-diagonal elastic constants. Their derivation for expressions relating non-diagonal elastic constants to 45° group velocities is not mathematically correct. The calculated off-diagonal stiffnesses by Cheadle et al. (1991) differ from the stiffnesses that would be calculated using their Thomsen anisotropy coefficients ($\epsilon, \delta and \gamma$ in Thomson (1986)). In this paper we present a method to determine all nine elastic constants of the phenolic LE material, that exhibits orthorhombic symmetry, using a set of group velocity measurements. A linear expression derived by Daley and Krebes (2006) between the P-wave group velocity in an arbitrary direction and elastic constants, has lead us to determination of all nine elastic constants.

We have utilized a physical modeling experiment to measure the group velocity in a number of different directions. The physical modeling is being carried out within the CREWES project at the University of Calgary. Our velocity measurements, with the shortest source-receiver distance more than six times the transducer's width, represent the group velocity in different directions. We implemented the acquisitions to measure the qP- and qS-wave velocities for different directions in 3D. The qP- and qS-wave velocity measurements along with the a linear expression between the qP-wave group velocity and elastic constants are employed in a least-squares inversion to calculate all nine elastic constants. In the experiment of determining all nine elastic constants, we found that the phenolic LE material exhibits seismic anisotropy very close to transverse isotropy, and the P-wave wavefront propagating through this material have the shape of an ellipsoid.

ORTHORHOMBIC SYMMETRY

Orthorhombic symmetry with three distinct directions is one of the simplest realistic symmetry systems for many geophysical problems. Fractures are commonly described by horizontal transverse isotropy (HTI) which is just a degenerated orthorhombic symmetry with only two distinctive directions. An orthorhombic model is characterized by three mutually orthogonal planes of mirror symmetry. In the cartesian coordinate system associated with the symmetry planes, the matrix of density normalized elastic constants ($A_{ij} = C_{ij}/\rho$) for orthorhombic symmetry is written as in Voigt notation

$$A_{\alpha\beta} = \begin{bmatrix} A_{11} & A_{12} & A_{13} & & & \\ A_{12} & A_{22} & A_{23} & & 0 & \\ A_{13} & A_{23} & A_{33} & & & \\ & & & A_{44} & & \\ & 0 & & & A_{55} & \\ & & & & & A_{66} \end{bmatrix}. \tag{1}$$

Describing an orthorhombic medium, nine independent density normalized elastic constants are required, ($A_{ii}, i = 1 : 6$) plus (A_{23}, A_{13}, A_{12}). The velocity measurements related to symmetry directions have simple expressions that allow particular elastic constants to be obtained. For an orthorhombic solid, taking the symmetry axes of the sample as principal axes, three P-wave velocities along principal axes determine the $A_{ii}(i = 1 : 3)$; three S-wave velocities also along the principal axes determine $A_{ii}(i = 4 : 6)$. The off-diagonal elastic constants (A_{23}, A_{13}, A_{12}) can not be determined from P-wave velocity measurements independently; they only can be determined in combination with other elastic constants. Generally, experimental determination of elastic constants is facilitated by the relation between the phase and group velocity with elastic constants of a medium. The next section discusses the phase expressions in terms of elastic constants.

Phase velocity expressions

The phase velocity, or wavefront velocity, is the velocity of seismic waves in the direction orthogonal to the wavefront. The theoretical equation for estimation of phase velocity in a general anisotropic homogeneous medium comes with solving the Christoffel equation (Schoenberg and Helbig, 1997; Tsvankin, 2001); see appendix A for derivation of phase velocity for orthorhombic symmetry.

The first-order linearized approximation for qP phase velocity in a weekly anisotropy medium is available in the literature for a range of disciplines of study (Backus, 1965; Every and Sachse, 1992; Daley and Krebes, 2006). The linear expression for qP phase velocity in geophysics discipline comes from the work of Backus (1965) as:

$$\rho v^2(\vec{n}) = c_{ijkl} n_i n_j n_k n_l \tag{2}$$

where ρ is density, the c_{ijkl} is $3 \times 3 \times 3 \times 3$ elastic constant tensor, v is the phase velocity, and $\vec{n} = (n_1, n_2, n_3)$ is a unit vector in the phase direction. Following Voigt's recipe the tensor c_{ijkl} will be represented by a 6×6 elastic constant matrix C_{ij}. Equation (2) for

orthorhombic symmetry reduces to (Every and Sachse, 1992; Daley and Krebes, 2006; Helbig, 1983)

$$\begin{aligned} v^2(\vec{n}) &= A_{11}n_1^4 + A_{22}n_2^4 + A_{33}n_3^4 + \\ & 2(A_{12}+2A_{66})n_1^2n_2^2 + 2(A_{13}+2A_{55})n_1^2n_3^2 + 2(A_{23}+2A_{44})n_2^2n_3^2 \end{aligned} \quad (3)$$

Following Daley and Krebes (2006) adding and subtracting the quantity

$$n_1^2n_2^2(A_{11}+A_{22}) + n_1^2n_3^2(A_{11}+A_{33}) + n_2^2n_3^2(A_{22}+A_{33}), \quad (4)$$

to equation (3), the following formula for phase velocity will result (Daley and Krebes, 2006),

$$v^2(\vec{n}) = A_{11}n_1^2 + A_{22}n_2^2 + A_{33}n_3^2 + E_{12}n_1^2n_2^2 + E_{13}n_1^2n_3^2 + E_{23}n_2^2n_3^2. \quad (5)$$

The quantities E_{ij} are the linearized forms of the anellipsoidal deviation terms, defined as

$$E_{13} = 2(A_{13}+2A_{55}) - (A_{11}+A_{33}), \quad (6)$$

$$E_{23} = 2(A_{23}+2A_{44}) - (A_{22}+A_{33}), \quad (7)$$

$$E_{12} = 2(A_{12}+2A_{66}) - (A_{11}+A_{22}). \quad (8)$$

The E_{13}, E_{23}, and E_{12} are anellipsoidal deviations terms in y-z, x-z, and x-y plane respectively. The exact anellipsoidal terms for the principal planes of x-z, y-z and x-y respectively can be defined as follows:

$$\tilde{E_{13}} = (A_{13}+A_{55})^2 - (A_{11}-A_{55})(A_{33}-C_{55}), \quad (9)$$

$$\tilde{E_{23}} = (A_{23}+A_{44})^2 - (A_{22}-A_{44})(A_{33}-C_{44}), \quad (10)$$

$$\tilde{E_{12}} = (A_{12}+A_{66})^2 - (A_{11}-A_{66})(A_{22}-C_{66}). \quad (11)$$

To clarify the meaning of the anellipsoidal deviation terms, elliptic anisotropy must be defined. Ellipsoidal anisotropy refers to the assumption regarding approximating the non-spherical wavefront in anisotropic media to an ellipsoid. There are many arguments about ellipsoidal anisotropy assumption in the geophysical literature. Thomson (1986) maintains that elliptical anisotropy is an inadequate approximation most of the time. Schoenberg and Helbig (1997) state that for transversely isotropic media, only the qSH wavefront is ellipsoidal; the qSV wavefront is never an ellipsoid, and the qP wavefront is an oblate ellipsoid (ellipsoid of revolution) if and only if the quantity $\tilde{E_{13}}$, defined perviously, vanishes.

It can be shown mathematically that the exact anellpisoidal deviation terms, $(\tilde{E_{13}}, \tilde{E_{23}}, \tilde{E_{12}})$ are the area difference the wavefront and associated ellipse. There for the exact anellipsoidal terms has the dimensions of squared velocity, so do their linear approximations (E_{13}, E_{23}, E_{12}).

The relation between the phase velocity and elastic constants, as in equation (3), has been used by many researchers (such as Every and Sachse (1992)) to invert for off-diagonal

elastic constants. However, the major problem is the fact that the measured velocity from traveltime data is group velocity and not phase velocity. Unfortunately, group velocity direction is not, in general, the same as the wavefront normal or phase velocity direction; only for extreme directions (including vertical or horizontal propagation) does group velocity equals phase velocity, see Appendix A. We can not make the simple substitutions of group velocity into equation (3) for all directions. In fact the accurate way to invert for elastic constants will be to use the relation between the group velocity and elastic constants. In this paper, we aim to determine the phenolic LE elastic constants from qP and qS travel time data based on the relation between group velocity and elastic constants. For simplicity, the qP and two qS-waves is refered to as only P- and S-waves throughout this report.

Group velocity

Figure 1 illustrates phase and group velocity in a homogeneous anisotropic medium. The group velocity is aligned with the source-receiver raypath, while the phase velocity (or slowness) vector is orthogonal to the wavefront. Group velocity, or ray velocity, determines the direction and speed of energy propagation. The slowness vector, $\vec{p}$, refered to as phase-velocity slowness, is defined as $\vec{p} = \vec{n}/v$. Plotting the phase velocity of a given mode as

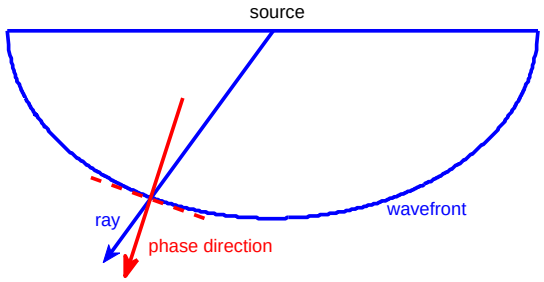

FIG. 1: The wavefront and group (ray) and phase direction in a homogeneous anisotropic medium.

the radius-vector in all directions defines the phase-velocity surface. Likewise, plotting the inverse value in the same fashion results in slowness surface. As discussed in Musgrave (1970), Helbig (1983), and Červený (2001) the group velocity direction is orthogonal to the slowness surface; also the slowness vector is perpendicular to the group-velocity surface. A careful examination of the group velocity surface reveals that the group velocity surface is actually displaying the wavefront at unit time, hence the normal to it determines the direction of the slowness vector. This property has been used to drive the expression defining the group velocity from the already known relation of the phase velocity (equation (3)).

For a material with elliptic anisotropy, for the slowness direction $\vec{p} = \vec{n}/v = (n_1/v, n_2/v, n_3/v)$, and the group velocity direction, $\vec{\xi} = \vec{N} = (N_1, N_2, N_3)$, the projection of slowness surface in principal plane of x-y plane will have the form

$$v^2(\vec{n}) = A_{11}n_1^2 + A_{22}n_2^2. \tag{12}$$

Musgrave (1970) (equations 8.2.1 and 8.2.2b page 96) using the orthogonality between the slowness surface and group velocity surface proved that the group velocity surface in x-y

plane has the form of

$$\frac{1}{V^2(\vec{N})} = \frac{N_1^2}{A_{11}} + \frac{N_2^2}{A_{22}}. \tag{13}$$

where V is group velocity.

For a general (non-elliptical) orthorhombic medium, Daley and Krebes (2006) obtained a reasonably accurate expression for qP group velocity by manipulating the eikonal equation, considering the phase velocity expression as in equation (3). They obtained a general expression for qP group velocity in an orthorhombic medium as

$$\frac{1}{V^2(\vec{N})} \approx \frac{N_1^2}{A_{11}} + \frac{N_2^2}{A_{22}} + \frac{N_3^2}{A_{33}} - \frac{E_{12}N_1^2N_2^2}{A_{11}A_{22}} - \frac{E_{13}N_1^2N_3^2}{A_{11}A_{33}} - \frac{E_{23}N_2^2N_3^2}{A_{22}A_{33}}. \tag{14}$$

A specified set of the P- and S-wave group velocity measurements is elaborated to yield all nine elastic constants of an orthorhombic symmetry material. The measurements of P- and S-wave group velocities in principal directions determine the diagonal elastic constants A_{ii} as in Table 1, see appendix (A) for the derivations. Determining the off diagonal elastic constants of A_{ij}, the expression for group velocity (equation 14) given different P-wave group velocity measurements will be inverted for anellipsoidal deviation parameters (E_{23}, E_{13}, E_{12}). Finally, using relation between anellipsoidal deviation parameters and A_{ij}s, equation 8-7, the off diagonal A_{ij} will be determined.

Table 1: Relation between C_{ii} and P- and S-waves group velocity in principal directions

P-velocity along x-axis	V_{11}	$\sqrt{A_{11}}$
P-velocity along y-axis	V_{22}	$\sqrt{A_{22}}$
P-velocity along z-axis	V_{33}	$\sqrt{A_{33}}$
S-velocity polarized in y-axis, propagating along z-axis	$V_{23} = V_{32}$	$\sqrt{A_{23}}$
S-velocity polarized in x-axis, propagating along z-axis	$V_{13} = V_{31}$	$\sqrt{A_{13}}$
S-velocity polarized in x-axis, propagating along y-axis	$V_{12} = V_{21}$	$\sqrt{A_{12}}$

PHYSICAL MODELING EXPERIMENT

Many theoretical predictions of wave propagation phenomena can be tested in laboratory experiments. In particular physical modeling can be extremely useful in bridging the gap between theory and the complexities observed in field seismic data (Cheadle et al., 1991). The physical modeling system is designed to carry out simulated seismic surveys on scaled earth-models. Physical modeling experiments have been continuing at the CREWES Project for more than two decades now (Bland et al., 2006; Wong et al., 2008). Our physical modeling experiment has a scale ($1 : 10000$) for distance (1mm in model represents $100m$ in real earth), and scale of ($10000 : 1$) for frequency (1 MHZ in experiment represents seismic waves of 100 HZ). Also, the system is equipped with a robotic positioning system to accurately position source and receivers to within $1mm$ (Wong et al., 2008).

The physical modeling experiment has been done on a model of LE-grade phenolic material; the scaled seismic data is incorporated when estimating elastic parameters of the phenolic material. Phenolic LE material is composed of laminated sheets of linen fabric,

with alternating fabric sheets oriented approximately orthogonal to each other, bonded with phenolic resin, and has a density of $1.39\ kg/cm^3$; phenolic LE material is available commercially. Previous research carried out in physical modeling laboratory of the CREWES project has shown that the phenolic laminate exhibits seismic anisotropy with apparent orthorhombic symmetry (Cheadle et al., 1991; Brown et al., 1991). Observed shear-wave splitting and azimuthal variation of NMO-velocity in Cheadle et al. (1991) confirmed that the phenolic material is appropriate for orthorhombic symmetry evaluation. Brown et al. (1991) used transmission shot gathers recorded by physical modeling to confirm the observed group velocities from the scaled data only differ from exact theoretical values by a maximum of about 1 percent; in calculation of exact theoretical velocities they used the elastic parameters estimated by Cheadle et al. (1991).

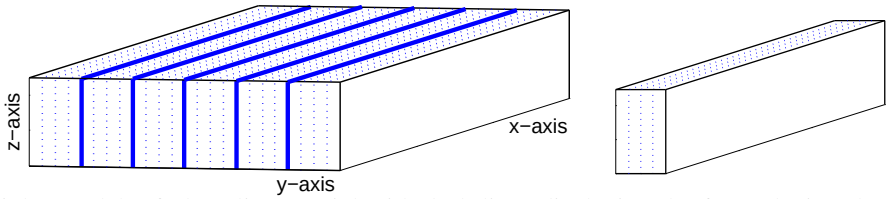

FIG. 2: (right) A slab of phenolic material with dash lines displaying the fast velocity plane. (left) The experimental model consisted of six slabs of phenolic glued on planes orthogonal to the symmetry axis (solid blue). Y-axis is the slow direction, and the x-z plane is the plane of fastest velocities.

Two boards of phenolic LE material measuring approximately $60cm \times 60cm$ with thickness of $6cm$ were purchased for this study. The sheets of linen fabric are laid horizontally so that a phenolic board resembles a VTI (vertical transverse isotropy) layer. To make a model that resembles an HTI layer the two phenolic boards were cut along planes orthogonal to the plane of linen layers. The first board was cut into six slabs; each slab was rotated 90° and glued together in the plane of linen fabric to make the model for this study. The second phenolic board was cut into 12 slabs to make a second model that will be used for future study. In total we had 18 phenolic slabs for which the P-wave velocity in three principal axes was measured in a simple ultrasonic transmission experiment conducted on each slab before gluing together, where just transmission time from the opposite sides of the slabs are measured. Table 2 (third column) shows the average of the P-wave velocity of the 18 phenolic slabs. Several repeated S-wave velocity measurements were done for only two of these slabs; the average of the S-wave velocity for the two slabs are as in Table 2 (third column).

In summary, the model for this study consists of six slabs of phenolic LE material glued together at their fast plane, to construct our sample fractured layer. Our model represents a natural fractured layer with an area of $5740m \times 5740m$ and a thickness of $701m$, where the x-z plane is the fracture plane (plane of fast velocities) and the y-axis is the symmetry axis (slow direction), see Figure 2. This report presents a new approach to estimate all required nine elastic parameters of the assumed orthorhombic symmetry for phenolic LE material.

Laboratory set up

The set-up of the laboratory equipment used in this report experiment is very similar to that described by Wong et al. (2008). Flat-faced piezoelectric cylindrical transducers are

used as both source and receivers in the physical modeling experiment; they convert electrical energy to mechanical energy and visa-versa. As a receiver, the P-transducer (Panametric V103) is sensitive to displacement normal to the contact face (acting as a vertical component geophone), and the S-transducer (Panametric V153) is sensitive to displacement tangential to the transducer (acting as horizontal component geophone); both transducers collect the particle displacement and convert it to electrical pulse. As a source both P- and S-transducers approximate a circular seismic array with far-field radiation patterns approximating those for normal and tangential displacement point sources (Aki and Richards, 1980). Both transducer generates both P- and S-waves, with the stronger generated P-wave from P-transducer and stronger S-wave from S-transducer along its polarization direction. We were able to record both wave types with both sources. Both P- and S-transducer have diameter of $13mm$, with central frequency of $1.0MHZ$. Data are recorded using a sampling interval of $1ms$.

Group velocity from transmission shot gathers

The linear P-wave group velocity expression (equation 14) is least-square inverted to yield the off diagonal elastic constants of the phenolic LE model. The group velocity measurements come from picking firstbreak traveltimes representing the direct arrival in a transmission shot gather, where the source and receivers are located on opposite sides of the phenolic model or the source and receivers at the same side of the model with the source in a vertical distance from the receiver profile. In these shot gathers the traveltime of the direct arrival from the source to each individual receiver gives the group velocity in the direction of the source-receiver raypath.

Receiver profiles initially located along the x- and y-axis at the top face of model (see Figure 3-top), with source at the bottom face gives group velocities in different directions on the principal x-z and y-z planes. The group velocities of the x-y plane are measured from receiver profiles along the x- and y-axis at the top surface with the source also at the top surface (see Figure 3-middle), with the source-receiver vertical distance of 1000 m. Additionally, the receiver profiles along $\pm 45^\circ$ azimuth line in the x-y plane provide group velocities in $\pm 45^\circ$ azimuth planes as illustrated in Figure 3-bottom.

Considering our model as a homogeneous layer, the source-receiver ray path is a straight line connecting them. Knowing the coordinates of source and receivers, the path length and angle of incidence are determined using basic trigonometry; the firstbreak pick of every trace gives the group velocity for the direction of the ray path connecting the source to that receiver. Note, the effective path length is, in fact, shorter than the nominal distance between transducer centers. The piezoelectric transducer generates the seismic waves along its entire element width. Hence elective path length equals to the distance between nearest edges of transducer (the nominal element size is considered to define the edge of the transducer). With the P-data dominant frequency of $30HZ$ and the picking error of one eighth of the dominant wavelength, the firstbreak picking has ± 0.004 s error. Consequently the calculated P-wave group velocity with $\pm 1mm$ error in receiver positioning has ± 25 m/s error. Similarly, with the dominant frequency of $10HZ$ for the S-data, the S-wave group velocity has $\pm 10m/s$ error. The firstbreak picking was done on raw data, whose only had trace normalization to boost the firstbreaks.

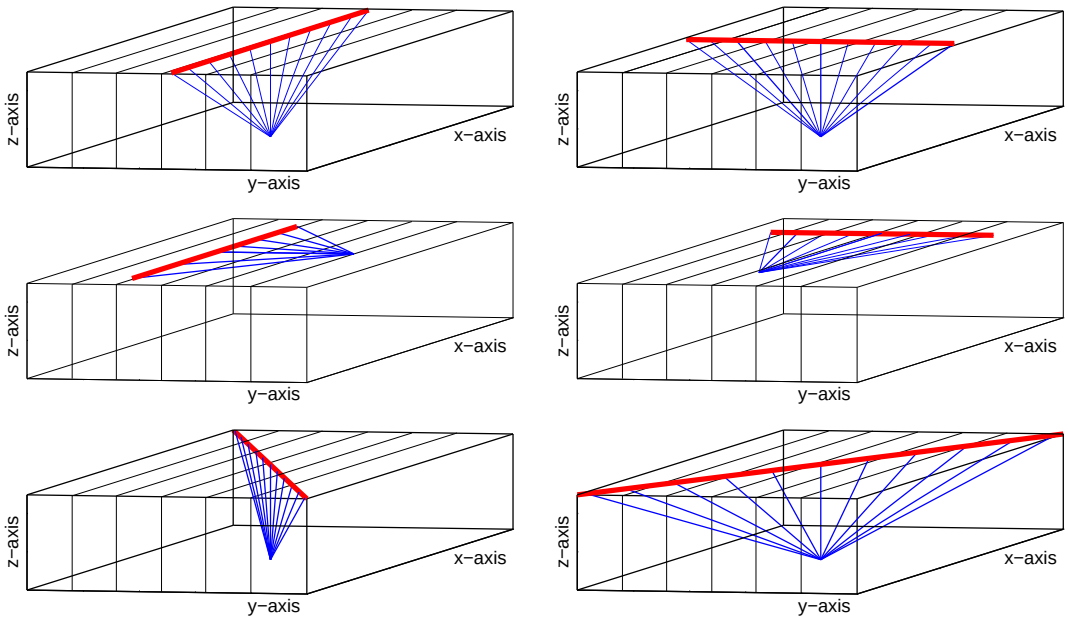

FIG. 3: Receiver profiles. (top left) Receiver profile along x-axis to measure group velocity in x-y plane. (top right) Receiver profile along y-axis to measure group velocity in y-z plane. (middle left) Receiver profile along x-axis to measure group velocity in x-y plane. (middle right) Receiver profile along y-axis to measure group velocity in x-y plane. (bottom left) Receiver profile along azimuth -45°. (bottom right) Receiver profile along azimuth +45°.

This experiment has been applied on the vertical component data acquired by using the P-transducers as both the source and receiver to provide the P-wave group velocity, followed by radial and transverse component data to obtain S-waves group velocity.

P-wave group velocity

Utilizing P-transducers as both source and receivers has enabled measurement of P-wave group velocities for different directions in three principal planes. Figure 4 shows the vertical component data of the transmission shot gathers for receiver profiles shown in Figure 3.

As discussed earlier, regardless of the type of transducer that was used as the source, both P-wave and S-waves are generated. The vertical component data recorded by P-transducers as the receiver, contains both P-wave and Sv-waves. Only, the Sv-wave does not appear in zero-offset or some near offset traces (Figure 4-top). With the P-transducer as the source the radial component data, recorded by radially polarized S-transducers as the receiver, also contains both P-wave and Sv-wave; but this time the P-wave does not appear in near-offset traces (Figure 11). Brown et al. (1991) implemented the P- and S-transducer as source and receivers (nine component data) and show clearly (their Figure 8) that the P- and S-waves are generated using both types of transducers. Note the discontinuity due to the contact faces of the six glued phenolic slabs, appears as a seam in the study model, has caused some diffractions specially in y-profile data (Figure 4-top left) which is marked in the Figure. A polar graph of the P-wave group velocity versus group angle (angle of the ray connecting source to receiver, here incident angle) provides the group velocity surface. The

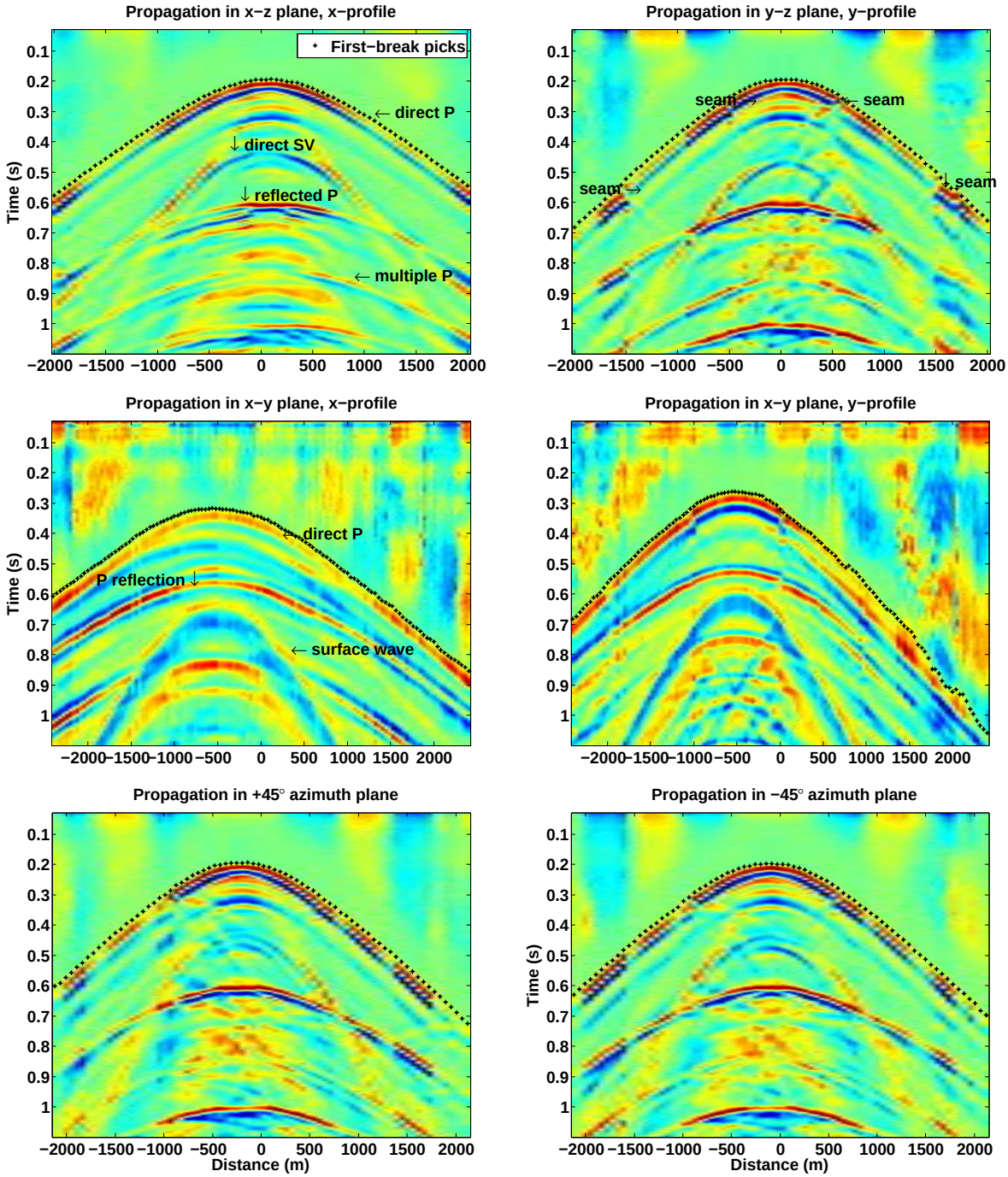

FIG. 4: Vertical component data of the shot gathers of Figure 3 profiles. Data has been filtered to [2 40] HZ, and AGC'ed with 400 ms window.

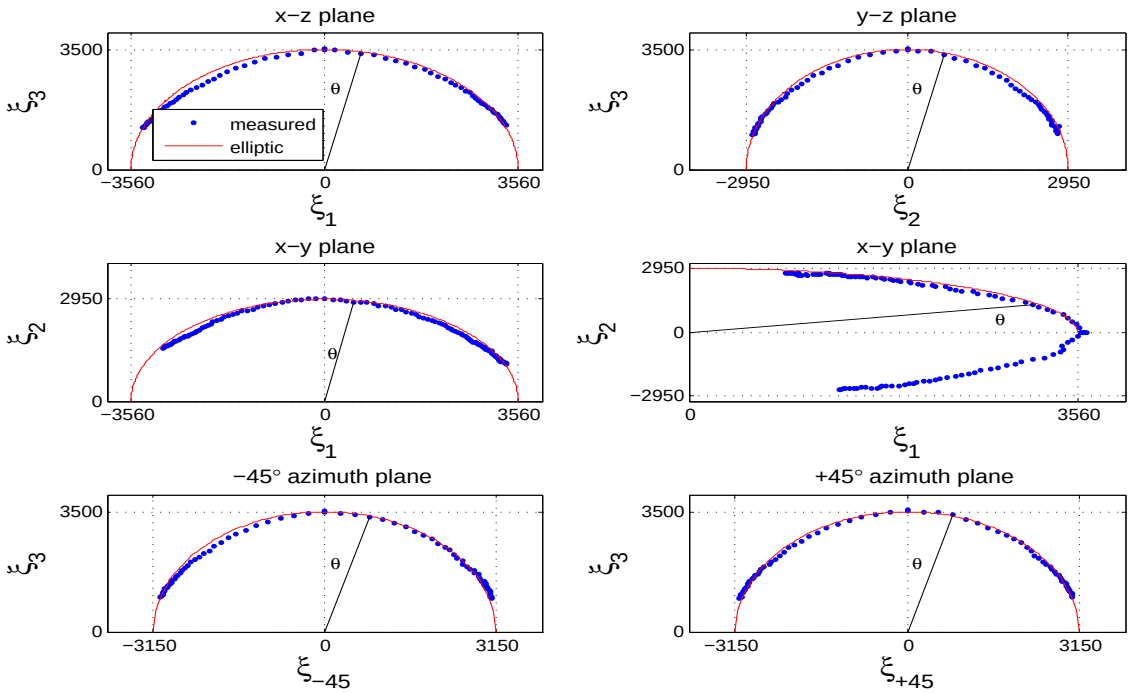

FIG. 5: The polar graph of group velocity surface versus group angle from firstbreak measurements of transmission shots gathers of Figure (4). (top and bottom) The incident angle is the angle of ray connecting source-receiver with z-axis. (middle) The incident angle with y-axis. For each plane the velocity read from firstbreak picking for the zero and 90° directions, are considered as the major and minor axes of the ellipse; using equation of an ellipse with known major and minor axes, the ellipse is plotted for each case.

group velocity surface for principal planes of x-z, y-z, x-y and also azimuth $\pm 45^\circ$ planes is illustrated in Figure 5. The measured P-wave velocity in the principal directions of the x- and y- and z-axis are 3560 (m/s), 3500 (m/s) and 2950 (m/s) respectively. These values are compared to an average of the measured velocities from a simple ultrasonic transmission experiment conducted on the 18 phenolic slabs. Comparing the third and forth column of Table 2 shows that group velocity calculated from firstbreak picks is well estimated.

A group velocity surface is, in fact, a wavefront at unit time. To examine how elliptical anisotropy assumptions can describe our phenolic material, an elliptical wavefront was plotted for each plane. In Figure 5 the group velocity measured from firstbreak picking is displayed by blue dots and the ellipse is displayed in red. For each plane the velocity read from firstbreak picking for the zero and 90° directions, are considered as the major and minor axes of the ellipse; using equation of an ellipse with known major and minor axes, the ellipse is plotted for each case. For example, for principal planes the major and minor axis of the ellipse are from measured group velocity in principal directions. Figure 6 shows the P-group velocity versus group angle (equal to incident angle here).

Comparing the ellipse to measured group velocity for each case indicates whether the elliptical anisotropy is adequate or not to describe the phenolic material anisotropy. For the y-z and x-y planes, the group velocity surface almost follows the ellipse perfectly whereas for the x-z plane there is a small deviation from ellipticity. In the x-z plane, the plane of fast velocities (fracture plane), a close match of group velocity to ellipse was expected; however, since the phenolic model is not a pure HTI medium and due to some inhomo-

geneity minor deviation from ellipse is observed. For the x-z plane examining the P-wave velocity versus incident angle (Figure 6) shows the variation of the velocity for this fast velocity plane; which can be considered as the cause of mentioned minor deviation in x-z plane. For the y-z and x-y planes, which are the planes containing slow-direction (y-axis), such a close match to ellipse was rather surprising, and more deviation from ellipticity was expected. The group velocity surface of the x-y plane, measured from the x-profile (Figure 5-middle left) and y-profile (Figure 5-middle right) are plotted on top of each other to examine the ties of the two plots, see Figure 8-left.

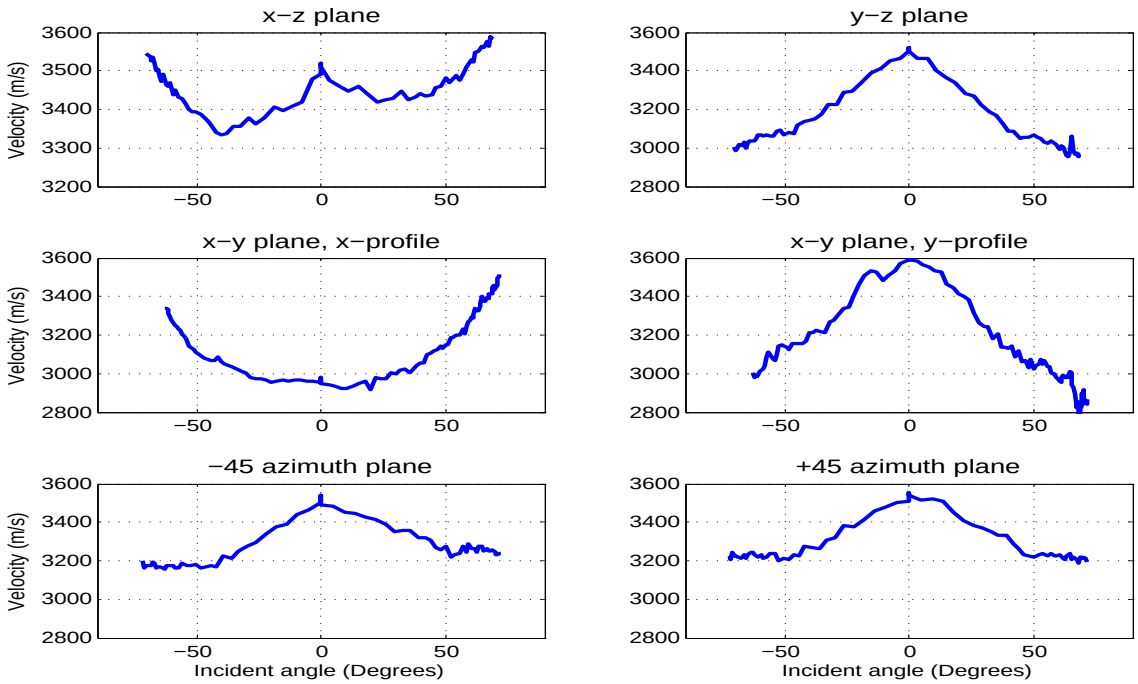

FIG. 6: P-wave group velocity versus incident angle. (top and bottom) The incident angle is the angle of ray connecting source-receiver with z-axis. (middle left) Incident angle with y-axis, (middle right) Incident angle with x-axis.

Table 2: P- and S-velocity in principal directions

Velocity	Slab measurements	Firstbreak picks
V_{11}	3542 ± 77	3560 ± 25
V_{22}	2926 ± 74	2950 ± 25
V_{33}	3425 ± 80	3500 ± 25
V_{23}	1525 ± 10	1530 ± 10
V_{13}	1670 ± 20	1700 ± 10
V_{12}	1500 ± 15	1510 ± 10

The group velocity surface of the x-y plane, measured from the x-profile (Figure 5-middle left) and y-profile (Figure 5-middle right) are plotted on top of each other to examine the ties of the two plots, see Figure 8 left. To confirm the observed elliptical anisotropy of the x-y plane, we conducted another experiment to obtain the group velocity surface. Seventeen reflection shot-gathers with receivers at 0°, ±14°, ±27°, ±37°, ±45°, ±53°, ±63°, ±76°, and ±90 ° azimuth were acquired with the source and receivers at the x-y plane (top face of our model). Figure 7 shows these azimuth profiles on the top face of

the phenolic model. In each azimuth reflection data, the dip of the firstbreak event (related to direct arrival from source to receivers on that azimuth) in the reflection data gives the group velocity along that azimuth; in each individual shot the firstbreak event is picked for all traces, then least-squares fitting gives the fist-break fitted line and the slope of it gives the velocity of that particular azimuth. The seventeen reflection azimuth data (vertical component data) are shown in Figures 9 and 10. A polar graph of measured velocity for these seventeenth azimuth data versus azimuth angle is depicted in Figure 8 at the top velocity measurements from the transmission experiment. Figure 8 left shows the group velocity surface in the x-y plane extracted from azimuth reflection data and confirms the elliptical anisotropy in x-y plane that we observed before from firstbreak picking of the transmission shot gathers; these two group velocities of the x-y plane are displayed in one plot to confirm the good match to elliptical anisotropy, see Figure 8.

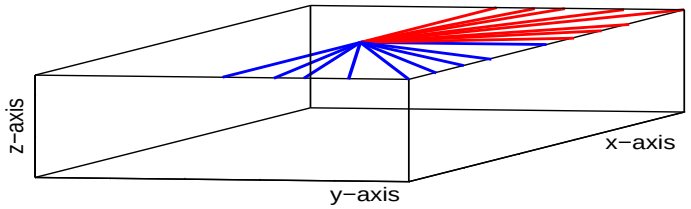

FIG. 7: Azimuth profiles to get the group velocity of x-y plane. Zero and positive azimuth profiles in red and negetive azimuth profiles in blue.

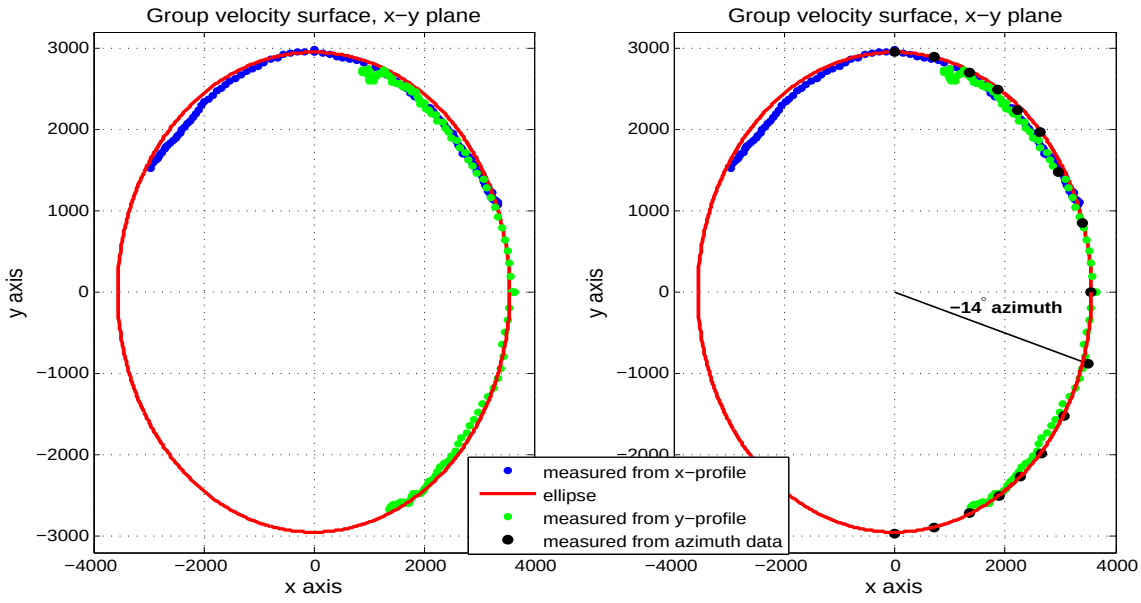

FIG. 8: (left) The group velocity surface of the x-y plane from the transmission shot gathers; blue dots are measured from x-profile data, green dots are measured from y-profile data, and the black dots are measured from azimuth data. The group velocity measured from the seventeen azimuth data are displayed at corresponding azimuths.

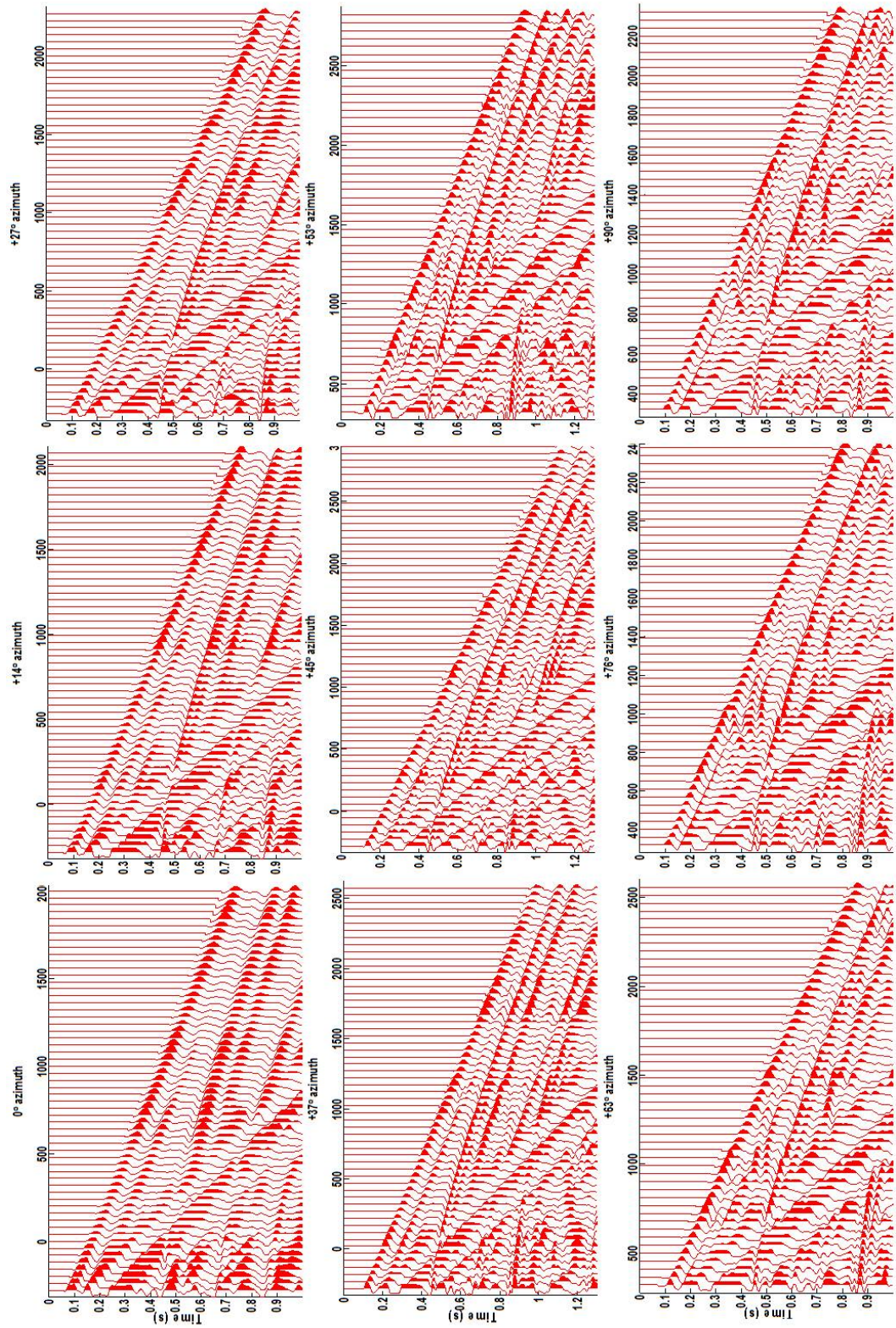

FIG. 9: Nine reflection shot-gathers with receivers at 0°, 14°, 27°, 37°, 45°, 53°, 63°, 76°, and 90 ° azimuth. Displayed data has been muted, AGCed and filtered to [0 4 50 100].

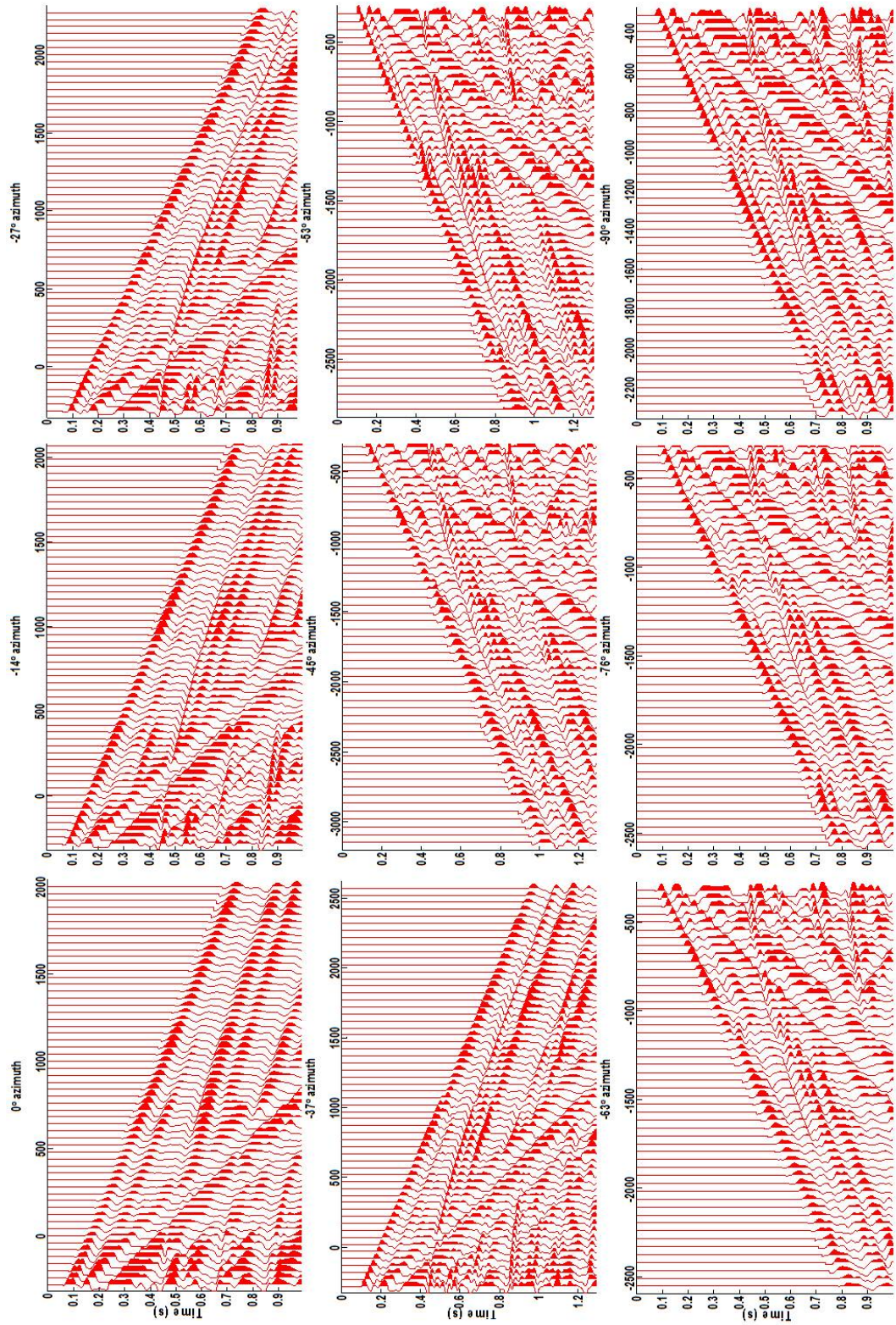

FIG. 10: Nine reflection shot-gathers with receivers at 0°, -14°, -27°, -37°, -45°, -53°, -63°, -76°, and -90 ° azimuth. Data has been muted, AGCed and filtered to [0 4 50 100].

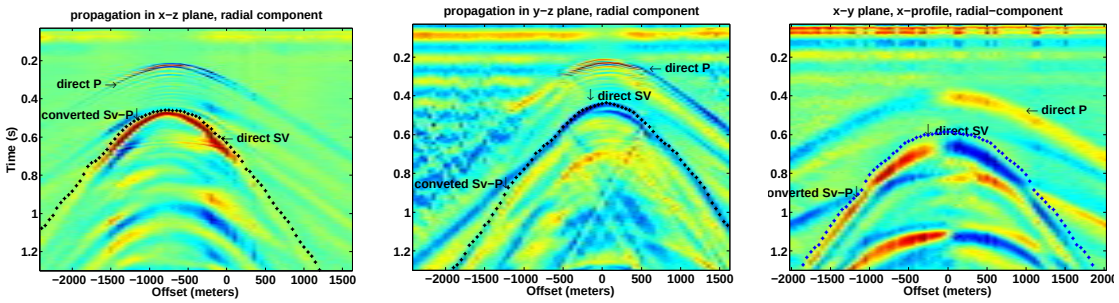

FIG. 11: The radial component of shots gathers of Figure 3 profiles. Firstbreak picks are depicted by black stars. Displayed data has been filtered to [2 40] HZ, and AGC'ed with 1400 ms window. The SV-wave after hitting the surface, is converted to the P- compressional wave, which is detected by the radial-component as shown in the section by "converted Sv-P" event.

S-wave group velocity

The ability to measure S-wave velocities in the laboratory significantly expanded the scope of issues we could explore in natural materials. The S-waves group velocity surfaces in the principal planes are examined. The S-waves wavefronts in the principal planes provide useful information on examining the orthorhombic symmetry material. Only the S-wave velocity in the principal directions (V_{23}, V_{13}, and V_{12}) will be used in our study to determine elastic constants of the phenolic model.

Using an experimental procedure similar to that described for measuring the P-wave velocity, for receiver profiles as in Figure 3 (top row and middle-left) radial and transverse component data was acquired. The radial component data is acquired using the radially polarized S-transducer, and the transverse component data is acquired using the transversely polarized S-transducer as the receivers. Figure 11 and 12 show the radial- and transverse component data. The vertical component data (Figure 4) seems noisier compared to horizontal component data (Figure 11 and 12) due to utilizing the amplifier in acquisition process; the amplifier has boosted the noise level.

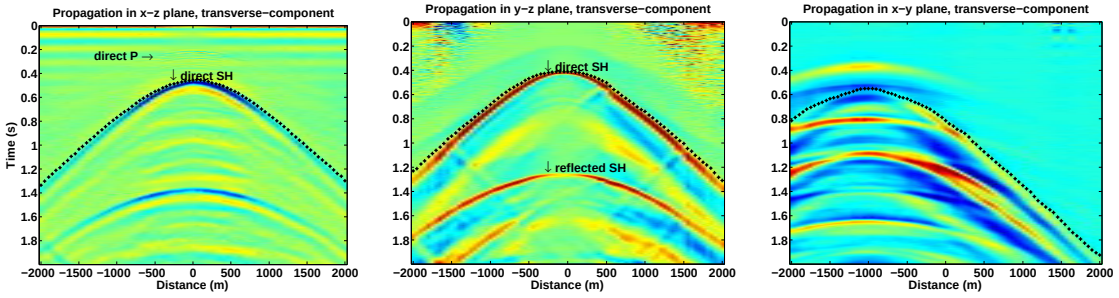

FIG. 12: Transverse component of shots gathers of Figure 3 profiles. First break picks are depicted by black stars. Displayed data has been filtered to [2 40] HZ, and AGC'ed with 1400 ms window.

With a similar procedure to the P-wave, S-wave group velocity in different directions were measured; the SV and SH-wave group velocity surfaces were examined, Figure 13. The SV-wave group velocity is measured from the first arrival traveltimes of the radial component data (11), and SH-wave group velocity is measured from transverse component data (12). Similar to the P-wave group velocity, compering the ellipse to the S-waves group velocity surfaces show that elliptical anisotropy is very good approximation for anisotropy

of the experimented phenolic material (Figure 11 and 12). Figure 11 shows that the Sv

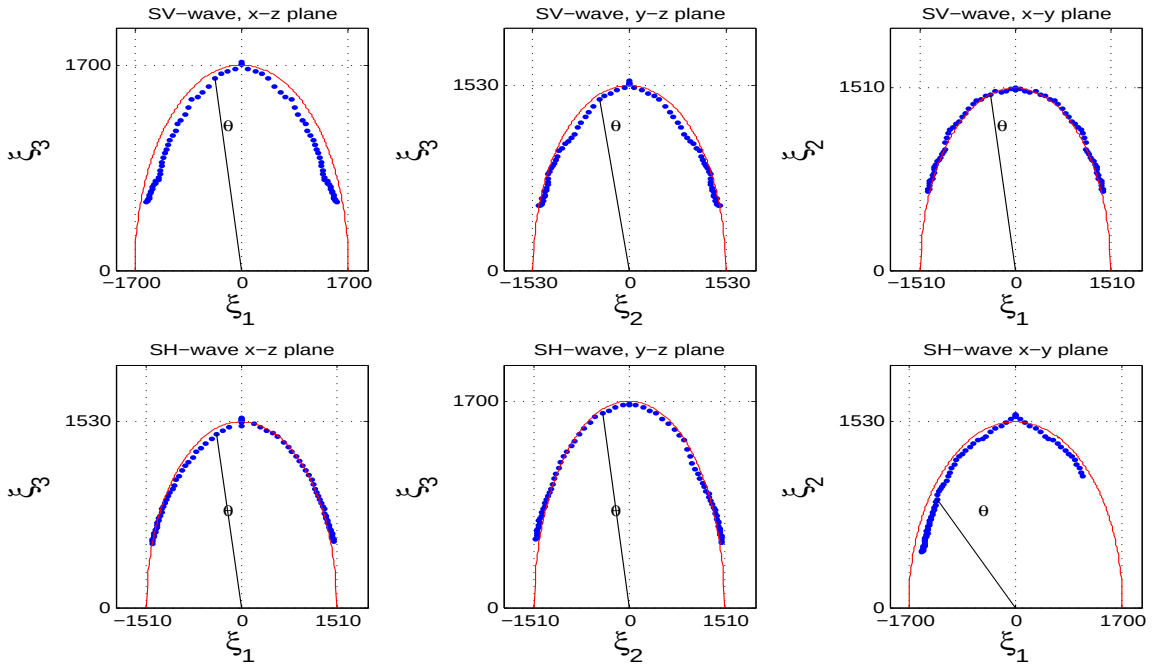

FIG. 13: (top) The polar graph of SV-wave group velocity surface versus group angle. (bottom) The polar graph of SH-wave group velocity surface versus group angle

group velocity surface is very close to a circle as $V_{Sv}(\theta) \cong V_{Sv}(\theta = 0)$; hence the kinematic of Sv-wave is not very influenced by anisotropy. The close match to ellipse for the SH-wave was expected, as for the SH wave in transverse isotropy medium always shows the elliptical anisotropy (Tsvankin, 2001).

In summary, the P- and S-waves velocity surfaces for the principal planes of x-z, y-z, and x-y are illustrated in Figure 14.

Determination of elastic constants of the phenolic model

The diagonal elastic constants is directly determined from the P- and S-waves measurements along the principal axes shown in Table 1, see Appendix A for the derivation. To determine the off diagonal elastic constants, as discussed earlier in this report, the linear relation between the P-wave group velocity and anellipsoidal deviation terms (E_{23}, E_{13}, E_{12}) is elaborated. Knowing the values of A_{11}, A_{22}, and A_{33}, the redundant measurements of P-wave velocity becomes the data vector in a least-squares inversion to estimate the E_{23}, E_{13}, and E_{12} values. The P-wave measurements from the transmission experiments can be inverted for the three unknowns using linear equation 14. For the P-wave propagation in the direction of $\vec{N} = (N_1, N_2, N_3)$ linear equation 14 can be written as

$$BE_{23} + FE_{13} + LE_{12} = D. \tag{15}$$

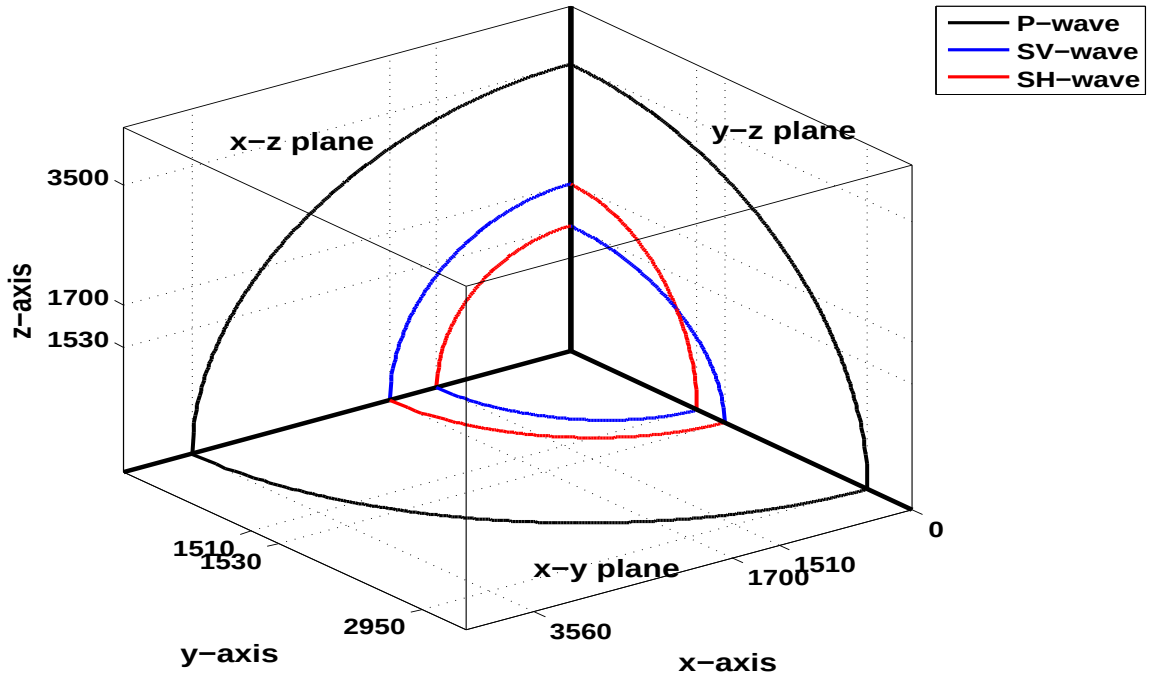

FIG. 14: The illustration of the P- and S-waves group velocity surfaces of the phenolic model.

The coefficeints D, B, F, L are defined as follows

$$\begin{aligned} D &= (\frac{{N_1}^2}{A_{11}} + \frac{{N_2}^2}{A_{22}} + \frac{{N_3}^2}{A_{33}}) - \frac{1}{V(\vec{N})^2}, \\ B &= \frac{{N_2}^2 {N_3}^2}{A_{22}A_{33}}, \\ F &= \frac{{N_1}^2 {N_3}^2}{A_{11}A_{33}}, \\ L &= \frac{{N_1}^2 {N_2}^2}{A_{11}A_{22}}. \end{aligned} \tag{16}$$

Incorporating n P-wave measurements, the linear equation 15 can be used to express a linear system of n equations with three unknowns:

$$\begin{pmatrix} B_1 & F_1 & L_1 \\ \vdots & \vdots & \vdots \\ B_n & F_n & L_n \end{pmatrix} \begin{pmatrix} E_{23} \\ E_{13} \\ E_{12} \end{pmatrix} = \begin{pmatrix} D_1 \\ \vdots \\ D_n \end{pmatrix}. \tag{17}$$

Or in a matrix form, $GE = D$. The unknown vector E will result from a damped least-squares inversion, as $E = (G^T G + \mu)^{-1} G^T D$ where the μ is the damping factor. The

Table 3: Normalized anellipsoidal deviation terms for phenolic LE model. As they have been normalized to A_{22}, they are dimensionless.

E_{23}/A_{22}	E_{13}/A_{22}	E_{12}/A_{22}
-0.132	-0.556	-0.261

phenolic LE material showed the anisotropy rather close to elliptical anisotropy; thus, we

expect to obtain very small relative deviation terms. The P-wave velocity measured in different directions of the x-z, y-z, x-y and $\pm 45^{\circ}$ planes are used as data in this least-squares inversion. The normalized anellipsoidal deviation terms resulted from the least-squares inversion are $-0.132, -0.556$, and -0.261 for E_{23}, E_{13}, and E_{12} respectively, as listed in Table 3. As we observed before from the P-wave group velocity surfaces, a higher deviation term (E_{13}) for the plane x-z was estimated, and the y-z and x-y planes have similar small divination terms. Finally using equations 8-7, the off diagonal density normalized elastic constants are calculated. Table 4 shows all nine density normalized elastic constants of the phenolic LE model.

Table 4: Density normalized elastic constants of the phenolic LE model. The A_{ij} have the units of $(km/s)^2$.

12.67 ± 0.006	6.13 ± 0.003	6.68 ± 0.003	0	0	0
	8.70 ± 0.006	5.79 ± 0.003	0	0	0
		12.25 ± 0.006	0	0	0
			2.34 ± 0.001	0	0
				2.89 ± 0.001	0
					2.28 ± 0.001

Having three very small deviation terms, all three deviation terms can be set to zero in estimation of off-diagonal elastic constants. All E_{23}, E_{13}, and E_{12} were set to zero, the nine density normalized elastic constants are calculated; there were almost no change in estimation values of off-diagonal elastic constants. Therefore, we conclude that only six diagonal elastic constants are enough in characterizing the phenolic LE model.

Since the strength of anisotropy is hidden in the elastic constants, we need to calculate the Thomsen anisotropy parameters. Now that all nine elastic constants of the phenolic LE material are determined, the Thomsen anisotropy coefficients $(\epsilon, \delta, \gamma)$ can be calculated; the conventional measures of anisotropy for the transverse isotropy case are given by Thomson (1986). The dimensionless Thomsen parameters (Thomson, 1986) which characterize the anisotropy of a medium are industry standard and is used in many commercial software. The dimensionless Thomsen parameters for an orthorhombic symmetry are given by Tsvankin (2001). Following Rüger (2001), the relationship between elastic constants to generic Thomsen parameters (for the principal planes of x-z, y-z, and x-y) are as in Table 5. Note, the calculated Thomsen parameters are exact values valid for any strength of anisotropy, which is different from week-anisotropy Thomsen parameters introduced by Thomson (1986). The small values of Thomsen parameters shows that the phenolic model has week anisotropy with $\epsilon \cong \delta$ for every principal planes (Table 5).

Table 5: The relationship between elastic constants to the generic Thomsen parameters. All the relations are valid for any strength of anisotropy.

Thomsen parameter	ϵ	γ	δ
x-z plane	$\frac{A_{11}-A_{33}}{2A_{33}}$	$\frac{A_{66}-A_{44}}{2A_{44}}$	$\frac{(A_{13}+A_{55})^2-(A_{33}-A_{55})^2}{2A_{33}(A_{33}-A_{55})}$
y-z plane	$\frac{A_{22}-A_{33}}{2A_{33}}$	$\frac{A_{66}-A_{55}}{2A_{55}}$	$\frac{(A_{23}+A_{44})^2-(A_{33}-A_{44})^2}{2A_{33}(A_{33}-A_{44})}$
x-y plane	$\frac{A_{22}-A_{11}}{2A_{11}}$	$\frac{A_{55}-A_{44}}{2A_{44}}$	$\frac{(A_{12}+A_{66})^2-(A_{11}-A_{66})^2}{2A_{11}(A_{11}-A_{66})}$

Table 6: Measured Thomsen anisotropy parameters.

	ϵ	γ	δ
x-z plane	0.0173	-0.0130	0.0175
y-z plane	-0.1448	-0.1055	-0.1318
x-y plane	-0.1567	0.1173	-0.1417

CONCLUSIONS

Employing the group velocity measurements, was a straightforward method in determining all nine elastic constants for a material with orthorhombic symmetry. Considering the transducer and a rock sample's dimensions, measuring the group velocity for different directions are easy and more reliable than the phase velocity measurements. With knowing the relation between the group velocity and all nine elastic constants in an orthorhombic material, this method can be applied in laboratory experiments as a robust method in determining all elastic constants of an orthorhombic material.

The P- and S-wave velocity examination of the physical modeling data showed that the phenolic LE material exhibits transverse anisotropy. The experimental model resembled a HTI layer or more accurately a vertically fractured transversely isotropic layer. Examining the P- and S-wave group velocity surfaces, revealed that the model has elliptic anisotropy for which the P- and S-wave have ellipsoidal wavefronts; therefore only six elastic constants are enough in characterizing the phenolic LE model. The Thomsen parameters values calculated from elastic constants, showed that the phenolic LE model has week anisotropy with very close values for the ϵ and δ parameters.

ACKNOWLEDGEMENTS

We thank the sponsors of CREWES for their crucial financial support and, in particular, acknowledge the support of the Canadian funding agencies NSERC and MITACS. Dr. Don Lawton is acknowledged for his guidance with the anisotropy concept as are Kevin Bertram for helping with slab velocity measurements, and Malcolm Bertram for his technical assistance in physical modeling. Faranak Mahmoudian wishes to thanks Dr. Mostafa Naghizadeh for helping in programming and preparing this report in Latex, Hassan Khaniani, and specially David Henley for many constructive discussions.

REFERENCES

Aki, K., and Richards, P. G., 1980, Quantitative seismology: Theory and methods, **vol 1**.

Auld, B. A., 1973, Acoustic fields and waves in solids, **vol 1**.

Backus, G. E., 1965, Possible forms of seismic anisotropy of the uppermost mantle under oceans.

Bland, H. C., Wong, J., Gallant, E. V., and Hall, K. W., 2006, Physical modeling: CREWES Report.

Brown, R., Lawton, D., and Cheadle, S., 1991, Scaled physical modeling of anisotropic wave propagation: multioffset profiles over an orthorhombic medium: Geophysical Journal International, **107**, 693–702.

Cheadle, S., Brown, R., and Lawton, D., 1991, Orthorhombic anisotropy:a physical seismic modeling study: Geophysics, **56**, No. 10, 1603–1613.

Daley, P. F., and Krebes, E., 2006, Quasi-compressinal group velocity approximation in a weakly anisotropic orthorhombic medium: Journal of Seismic Exploration, , No. 14, 319–334.

Dellinger, J., and Vernik, L., 1994, Do traveltimes in pulse-transmission experiments yield anisotropic group or phase velocities?: Geophysics, **59**, No. 11, 1774–1779.

Every, A., and Sachse, W., 1992, Sensetivity of inversion algorithms for recovering elastic constants of anisotropic solids from longitudinal wavespeed dara, 43–48.

Helbig, K., 1983, Elliptical anisotropy-its significance and meaning: Geophysics, **48**, No. 7, 825–832.

Jones, E. A., and Wang, H. F., 1981, Ultrasonic velocities in cretaceous shales from the williston basin: Geophysics, **21**, 905–938.

Lo, T. W., Coyner, K. B., and Toksoz, M. N., 1986, Experimental determination of elastic anisotropy of berea sandstone, chicopee shale, and chelmsford granite: Geophysics, **51**, 164–171.

Mah, M., and Schmitt, D. R., 2001, Experimental determination of the elastic coefficients of an orthorhombic material: Geophysics, **66**, No. 4, 1217–1225.

Mah, M., and Schmitt, D. R., 2002, Determination of the complete elastic stiffnesses from ultrasonic phas evelocity measurements: CSEG expended abstract.

Musgrave, M. J. P., 1970, Crystal acoustics.

Rüger, A., 2001, Reflection coefficeints and azimuthal avo analysis in anisotropic media.

Schoenberg, M., and Helbig, K., 1997, Orthorhombic media: Modeling elastic wave behavior in a vertically fractured earth: Geophysics, **62**, 1954–1974.

Thomson, L., 1986, Weak elastic anisotropy: Geophysics, **51**, No. 10, 1954–1966.

Tsvankin, I., 2001, Seismic signatures and analysis of reflection coefficients in anisotropic media.

Červený, V., 2001, Seiemic ray theory.

Vernik, L., and Nur, A., 1992, Ultrasonic velocity and anisotropy of hydrocarbon source-rocks: Geophysics, **57**, 727–735.

Vestrum, R. W., 1994, Group- and phase- velocity inversions for the general anisotropic stiffness tensor: M.Sc. thesis, Univ. of Calgary.

Vestrum, R. W., Lawton, D., and Schmid, R., 1999, Imaging structures below dipping ti media: Geophysics, , No. 64, 1239–1246.

Wong, J., Hall, K. W., Gallant, E. V., and Bertram, M. B., 2008, Mechanical and electronic design for the u of c seismic physical modelling facility: CREWES Report.

APPENDIX A

This appendix follows Cheadle et al. (1991) and Tsvankin (2001) to provide the relationship between elastic constants and phase velocity in an anisotropy medium of orthorhombic symmetry.

Christoffle equation describes the wavefront propagation in the direction of orthogonal (or phase direction) to wavefront. The velocity in the direction of the normal to wavefront, is known as phase velocity, v. If $\vec{n} = (n_1, n_2, n_3)$ to be the unit vector in phase direction, the slowness vector $\vec{p} = \vec{n}/v$. The phase velocity results from solving the Christoffle equation. The following briefly explains the derivation of Christoffle equation. Consider the elastic wave equation,

$$\rho(\partial^2 u_i/\partial t^2) = c_{ijkl}(\partial^2 u_i/\partial x_j \partial x_l). \tag{A-1}$$

Substitute a trial plane wave solution of

$$u_k = U_k e^{i\omega(n_j x_j/v - t)}, \tag{A-2}$$

(where $\vec{n}$ is normal to the wavefront, $\vec{U}$ is polarization vector) into the wave equation, which leads to the following system of equations

$$\begin{bmatrix} G_{11} - \rho v^2 & G_{12} & G_{13} \\ G_{21} & G_{22} - \rho v^2 & G_{23} \\ G_{31} & G_{32} & G_{22} - \rho v^2 \end{bmatrix} \begin{bmatrix} U_1 \\ U_2 \\ U_3 \end{bmatrix} = \begin{bmatrix} 0 \\ 0 \\ 0 \end{bmatrix}. \tag{A-3}$$

where $G_{ik} = C_{ijkl} n_j n_l$. The equation (A-3) that solves for the phase velocity, v, and polarization vector , U, is the known as the Christoffle equation (**?**Tsvankin, 2001).

The Christoffle equation describes a standard eigenvalue problem for the matrix G. The eigenvalues are found from setting the $\det\left[G_{ik} - \rho v^2 \delta_{ik}\right] = 0$. The symmetric matrix G is positive definite (Musgrave, 1970), therefore has three real positive eigenvalues, ρv^2. For an arbitrary slowness direction $\vec{n}$ in the anisotropic media, solving this determinant yields three possible values of phase velocity, which corresponds to one qP-wave and two qS-waves.

Solving equation (A-3) for an arbitrary wave propagation direction results in nonlinear expressions (with respect to elastic constants) for the three phase velocities. However for wave propagation along a principal direction, the equation (A-3) result in linear phase velocities that only depend on one diagonal element of elastic constants. As an example propagation in one principal direction is given.

Propagation along a principal direction

Following Cheadle et al. (1991) for propagation along the x-axis, equation (A-3) becomes:

$$\begin{bmatrix} A_{11} - v^2 & 0 & 0 \\ 0 & A_{66} - v^2 & 0 \\ 0 & 0 & A_{55} - v^2 \end{bmatrix} \begin{bmatrix} U_1 \\ U_2 \\ U_3 \end{bmatrix} = \begin{bmatrix} 0 \\ 0 \\ 0 \end{bmatrix}; \tag{A-4}$$

where the three eigenvalues of the above matrix are $v^2 = A_{11}$ related to P-wave polarized in x-axis, and $v^2 = A_{55}$, $v^2 = A_{66}$ related to S-waves polarized along z-axis and y-axis respectively. In other words, for the wave polarizing on the x-axis ($U_1 \neq 0$), the phase velocity will be $v = \sqrt{A_{11}}$; this describes P-wave propagating along x-axis with the velocity of V_{11}. Similarly, the wave polarized along the z-axis with the velocity of $v = \sqrt{A_{66}}$, is the S-wave propagating along the x-axis and polarized along z-axis with the velocity of V_{13}. For the third eigenvalue, the wave polarized along the y-axis with the velocity of $v = \sqrt{A_{55}}$

is the S-wave propagating along the x-axis and polarized along the y-axis with the velocity of V_{12}. For principal directions, and at other maxima or minima of the phase velocity, the group velocity and phase velocity coincides (Tsvankin, 2001); hence measurements of group velocity of P- and S-waves along the x-axis can result in knowledge of A_{11}, A_{55}, and A_{66} respectively. In a similar fashion, the other diagonal elastic constants A_{22}, A_{33}, and A_{44}, can be obtained from measurements of the group P-and S-waves velocities in other principal directions. Table (1) summarizes the diagonal elastic constants relations.

Linearizing the solutions of phase velocity has been done by numerous people see Backus (1965); Every and Sachse (1992); Daley and Krebes (2006) among others. The linearized P-wave phase velocity for orthorhombic symmetry has the form of (Tsvankin, 2001; Daley and Krebes, 2006)

$$\begin{aligned} \rho v^2 &= A_{11}n_1^4 + A_{22}n_2^4 + A_{33}n_3^4 + \\ &\quad 2(A_{12}+2A_{66})n_1^2n_2^2 + 2(A_{13}+2A_{55})n_1^2n_3^2 + 2(A_{23}+2A_{44})n_2^2n_3^2 \end{aligned} \tag{A-5}$$